Supporting information

Closed Bipolar Electrode Based Fluorescence Visualization Biosensor for Anti-interference Detection of T-2 toxin

Nan Hao[a*], Yu Qiu[a], Yaqi Li[d], Jinwen Lu[a], Xu Han[c], Jing Qian[a], Kun Wang[a,b*]

[a]School of Chemistry and Chemical Engineering, Jiangsu University, Zhenjiang 212013, PR China

[b]Key Laboratory of Sensor Analysis of Tumor Marker, Ministry of Education, College of Chemistry and Molecular Engineering, Qingdao University of Science and Technology, Qingdao 266042, PR China

[c]Science and Technology on Space Physics Laboratory, Beijing, 10076, PR China

[d]School of Grain Science and Technology, Jiangsu University of Science and Technology, Zhenjiang, 212003, China

E-mail address: hn@ujs.edu.cn; wangkun@ujs.edu.cn; Tel/Fax: +86 517 83559061; +86 511 88791800.

Experiment

Reagents and Chemicals.

Cs_2CO_3 (99.99%), PbI_2 (99.9%), octadecene (ODE, > 90%), oleic acid (OA, 85%), oleyl amine (OAm, 80-90%) were obtained from Aladdin (China). Tetrabutyl titanate (TBT), HF, Citric acid, Ethylenediamine, Urea, Bovine serum albumin (BSA), Powdery chitosan (CS), and N-hexane were obtained from Sigma-Aldrich. Silicone Elastomer Base (SYLGARD™ 184) was purchased from Dow Corning (USA). Indium tinoxide (ITO)-coated alum inosilicate glass slides were purchased from CSG (China). The de-signed aptamer for T-2 toxin with the following sequence: 5′-NH2 -GTAT ATCA AGCA TCGC GTGT TTAC ACAT GCGA GAGG TGAA-3′ was purchased from Sangon Biotech (China). Deionized water was purified by a Milli-Q system (MA). All chemicals were received without any further purification.

Apparatus.

UV–vis spectra was characterized by Shimadzu UV-2450 spectrophotometer (Japan). Fluorescence spectra was obtained on Hitachi F-4500 fluorescence spectra-photometer (Japan). X-ray diffraction (XRD) spectra was obtained through a Bruker D8ADVANCE instrument. Transmission Electron Microscopy (TEM) was performed on a JEOL 100 instrument (Japan). X-ray photoelectron spectrometry (XPS) analyses were measured by a VG MultiLab 2000 system. All the electrochemical experiments were conducted with a CHI760e electrochemical work-station (Shanghai Chenhua Instrument Corporation, China).

Preparation of CQDs.

The synthesis scheme of CQD was based on the literature[1] and modified as follows: 15.7605 g of citric acid and 5.025 ml of ethylenediamine were dissolved in 90 mL of deionized water, and the mixture solution was transferred to a Teflon-lined stainless-steel autoclave and kept at 180 °C for 6 h. After cooling to room temperature, the brown solution was dialyzed for 48 h, then freeze-dried for 12 h. Finally, the freeze-dried solid was washed with ethanol and deionized water, and then the CQDs solid was obtained by centrifugation.

Preparation of g-C_3N_4.

The g-C_3N_4 were prepared using urea as a carbon and nitrogen source according to previous reports.[2] In general, 9 g of urea was placed in an alumina crucible with a lid, heated in a tube furnace at a heating rate of 0.5 °C·min^{-1} to 550 °C, and calcined at this temperature for 3 hours. After cooling to room temperature, the obtained g-C_3N_4 was stirred in 5 mol·L^{-1} HCl for 6 hours, and the light-yellow g-C_3N_4 product was collected. Then the g-C_3N_4 sheets were obtained by washing with deionized water until the pH reached 7, and drying at 80 °C overnight.

Preparation of TiO_2 NSs.

TiO_2 nanosheets were prepared by hydrothermal method based on the literature.[3] In a typical preparation experiment, 50 ml of tetrabutyl titanate (TBT) and 6 ml of HF were mixed and magnetically stirred, and then transferred to a Teflon-lined stainless-steel autoclave for hydrothermal treatment at 180 °C for 24 hours. The obtained solution was first washed with NaOH solution to remove fluorine on the surface of

TiO_2, then washed with water and ethanol, finally the obtained precipitate was placed in an oven at 80 °C for 6 hours.

Preparation of $CsPbI_3$ QDs.

The $CsPbI_3$ (CPI) QDs sample was synthesized according to the reported method,[4] but modified as follow: Briefly, 2 mL OA and 2 mL OAm were added to a mixture containing 10 mL ODE and 0.174 g of PbI_2 after degassing for one hour and heated to 120 °C under N_2. The solid was completely dissolved and heated 150 °C. Then, 1.6 mL Cs-oleate solution (formed by heating 0.407 g Cs_2CO_3, 20 mL ODE and 1.25 mL OA to 150 °C under N_2) was added and the reaction was transferred to ice water bath after 5 seconds to stop the reaction. After purification by centrifugation, the solid was dispersed in n-hexane and protected from light.

Device Fabrication.

The patterning of ITO glass was the same as in reported work.[5] Briefly, the patterned screen-printing plate was covered on the surface of clean ITO glass, then the ink was brushed in the pattern area, and then baked at 80 °C for 15 minutes. Finally, the exposed ITO can be easily etched by an acidic etchant. And the patterned ITO electrode chip was obtained by removing the ink in the pattern area through a strong alkaline solution. The manufacturing process of PDMS membrane was as follows[6]: 20g of Silicone Elastomer Base (SYLGARD™ 184) and 2g of curing agent were added to a watch glass, stirred for 15 minutes, the bubbles were completely driven out by ultrasonic method, and then heated and cured at 70 °C for 1h. After cooling to room temperature, two reservoir layers (5 × 1 × 5 mm) were formed on the PDMS

membrane according to the patterned size. Finally, a closed BPE system was formed by bonding the PDMS reservoirs to a patterned ITO chip.

PB was electrodeposited onto the reporting cell by cyclic voltammetry from 0.8 V to 0.4 V within 600 s. Then the electrode was thoroughly rinsed and dried naturally. The ITO electrode coated with a PB film was then added with N-hexane solution containing 0.05 M CPI QDs, and after the N-hexane was evaporated to form a CPI QDs film, the PB/CPI QDs nanocomposite film modified electrode was obtained. The sensing cell was first modified with 20 μL CCNT composite (2 mg / mL), and allowed to stand at room temperature for 1 hour to form a transparent film. After adding 10 μL of chitosan solution and 10 μL of glutaraldehyde solution, 10 μL of T-2 toxin aptamer (2 μM) was modified on the surface of the electrode (sensing area) and incubated in a refrigerator at 4 °C for 10 h. After washed with deionized water and PBS, 10 μL of 3% BSA was added onto sensing area and reacted at 4 °C for 1 h.

Visualization method for T-2 toxin detection.

After the biosensor assembly was completed, the T-2 toxin solution with different concentrations were introduced into the sensing cell and incubated at 37 °C for 40 minutes. After washing twice with the PBS solution, 20 μL of the PBS solution was introduced into the sensing cell. 20 μL EA solution was added to the reporting cell, then the sensing area of the electrode was placed in the irradiation center of the Xenon lamp, and the power was turned on for 2 minutes. Photographs of fluorescence under the UV light of the reporting cell were collected via a mobile phone, and the data was processed with Photoshop software.

Results and Discussion

Material characterization

The SEM image and EDS (Fig. S1) further confirm the presence of g-C_3N_4 and TiO_2 in CCNT. Fig. S1A and B clearly show that TiO_2 NSs are deposited on the bulk g-C_3N_4, but no CQD is observed due to the small diameter. As shown in Fig. S1, four elements of C (C), N (D), O (E)and Ti (F) can be detected simultaneously in the CCNT samples.

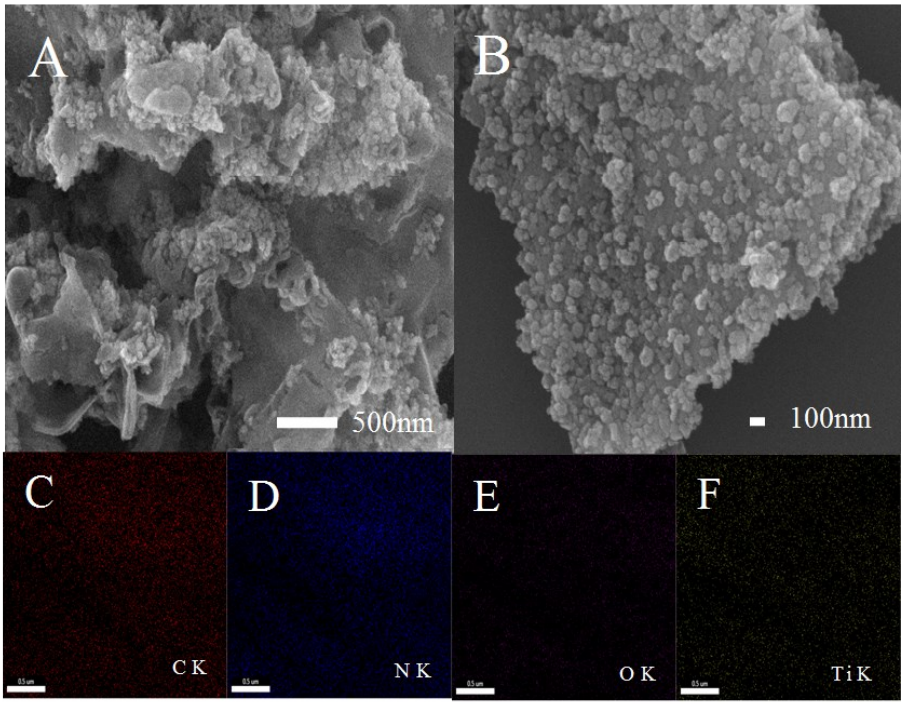

Fig. S1 (A, B) The SEM images of CCNT. EDS of multi-elemental map obtained from SEM: (C) C element map, (D) N element map, (E) O element map and (F) Ti element map.

The X-ray diffraction patterns of pure g-C_3N_4, pure TiO_2 NSs and CCNT are shown in Fig. S2A. For pure g-C_3N_4, the two diffraction peaks appearing at 27.4 ° and 13.1 ° belong to the (002) and (100) characteristic crystal planes of g-C_3N_4, respectively. For pure TiO_2 and CCNT samples, characteristic peaks appearing at 25.5

°, 37.9 °, 48.0 °, 54.3 °, 55.2 °, 62.7 °, 68.8 °, and 75.2 ° can be easily designated as the (101) (004), (200), (105), (211), (204), (116), and (215) crystal planes of anatase phase TiO_2.[7] In addition, the (002) crystal plane belonging to g-C_3N_4 is easily seen in the CCNT sample. Due to the low content and weak crystallinity, no characteristic peaks of CQD are found in CCNT samples. These results indicate that ternary composite photochromic materials have been successfully pre-pared. The UV-visible spectrum and PL spectrum of $CsPbI_3$ QDs are shown in Fig. S2B. Obviously, the $CsPbI_3$ QDs have a maximum absorption peak near 675 nm and a steep emission peak near 690 nm, which is consistent with previous reports.[8]

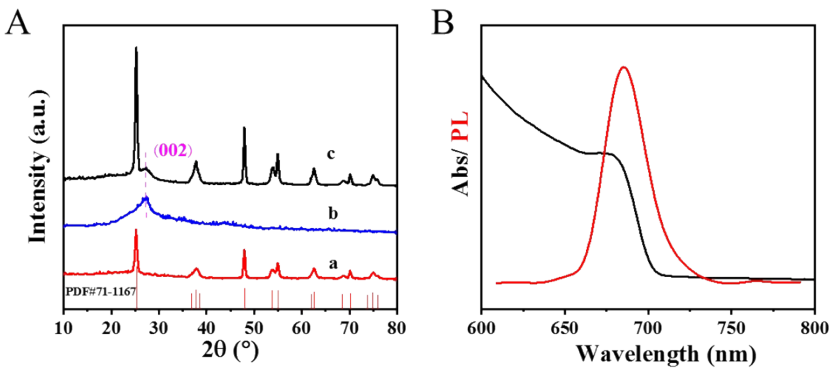

Fig. S2 (A) XRD patterns of synthetic CCNT, g-C_3N_4 and TiO_2 NSs. (B)UV−vis absorption and PL spectra of $CsPbI_3$ QDs in hexane.

In order to further explore the chemical structure of CCNT, X-ray photoelectron spectroscopy (XPS) analysis was performed. Fig. S3A shows the XPS survey spectrum of CCNT, in which C (288 eV), N (399 eV), Ti (458 eV) and O (530 eV) peaks are evident. In Fig. S3B, two singlet peaks can be observed at 285.3 and 288.4eV for C 1s, one is the standard carbon of the sample and the other is the typical sp^2-hybrid carbon in g-C_3N_4.[9] In Fig. S3C, the N 1s peak can be subdivided into four peaks of 398.9, 400.2, 401.4, and 404.7 eV, respectively. These four peaks are derived

from sp^2-hybrid nitrogen in the form of -C-N = C, N- $(C)_3$ group, uncondensed C-N-H functional groups on the surface, and charge effects in the heterocyclic ring.[10] Fig. S3D shows that the two peaks at 458.8 eV and 464.5 eV belong to the spin orbit split lines of Ti 2p3/2 and Ti 2p1/2, indicating that Ti 2p exists as Ti^{4+} in TiO_2. As shown in Fig. S3E, for O1s, the peak at 530 eV corresponds to the lattice oxygen of TiO_2, and at 531.4 eV corresponds to the surface hydroxide.[11]

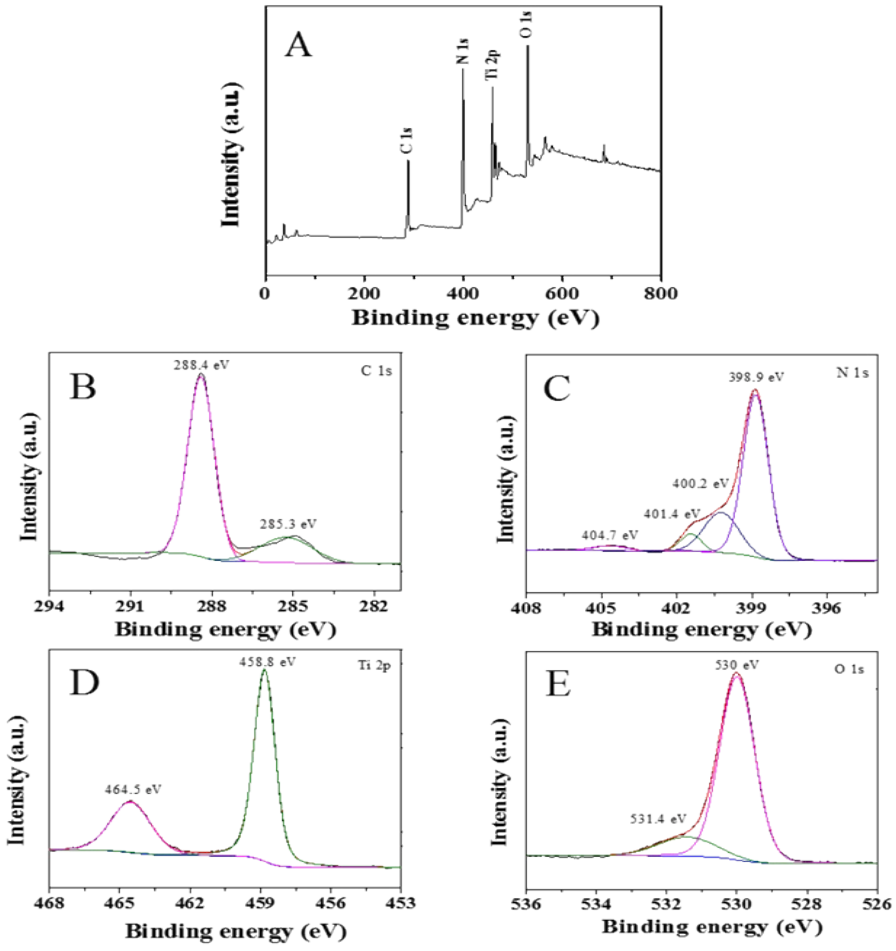

Fig. S3 (A) XPS survey spectrum of the CCNT sample and high-resolution XPS spectra of (B) C 1s, (C) N 1s, (D) Ti 2p and (E) O 1s for the CCNT sample.

Fig. S4A and S4B show the ultraviolet-visible diffuse reflection spectrum (DRS) and estimated band gap of TiO_2 NSs, g-C_3N_4 and CCNT. As shown in Fig. S4A, the curve of pure TiO_2 NSs (black line) have a significant increase at the wavelength of

395 nm, which is consistent with the inherent absorption edge of anatase TiO_2.[12] The calculated band gap of pure TiO_2 NSs is 3.26 eV (Fig. S4B), which result in low visible light utilization. The pure g-C_3N_4 curve (red line) also shows a significant increase at the 440 nm wavelength, and the calculated band gap is 2.9 eV (Fig. S4B). As shown in Fig. S4A, the CCNT composite (blue line) exhibit two intrinsic absorptions corresponding to pure TiO_2 and pure g-C_3N_4 in the range of 200 to 400 nm and 400 to 500 nm, respectively. In addition, CCNT composites have strong background absorption due to the presence of black CQD. The absorption wavelength (blue line) of CCNT composites extend into the visible light region (460 nm) and has a smaller band gap (2.80 eV), indicating that compared with TiO_2, CCNT composites improve the utilization of visible light.

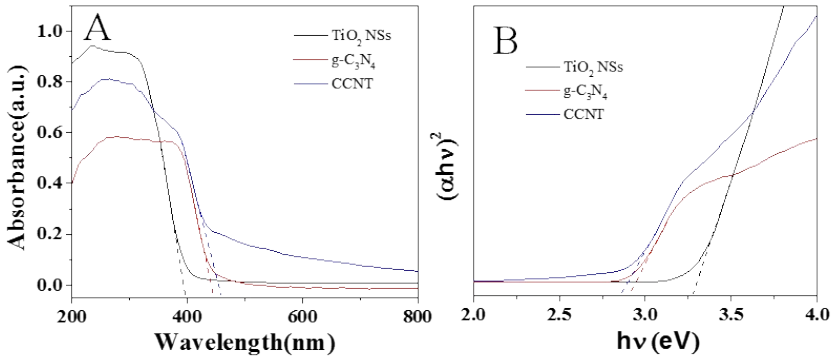

Fig. S4 (A) UV-vis absorption spectra and (B) the estimated band gap of TiO_2 NSs(black), g-C_3N_4 (red) and CCNT (blue).

The PEC test was performed in 0.1 M PBS under visible light. As shown in Fig. S5A, the photocurrents of pure g-C_3N_4 and pure CQD (curves a and b) are extremely small, while the photocurrents of pure TiO_2 NSs (curve c) are relatively large. The photocurrent intensity of g-C_3N_4 and TiO_2 NSs composite (CNT, curve d) is significantly higher than that of pure TiO_2 NSs. The photocurrent intensity (CCNT, curve e) is greatly improved after doping CQD in the CNT composite and the

photocurrent intensity is 64 times, 32 times, 3 times and 1.3 times of pure g-C_3N_4, pure CQD, pure TiO_2 and CNT composites, respectively. As shown in Fig. S5B, the Ret (semicircle portion) of CNT (curve d) is significantly smaller than that of pure g-C_3N_4 (curve a) and pure TiO_2 NSs (curve c), which may be attributed to the hetero-junction structure formed between g-C_3N_4 and TiO_2 effectively promoted electron transfer. In addition, the resistance value of CNT (curve d) is greater than that of CCNT (curve e), which indicate that the introduction of CQD further promoted electron transfer. The above results show that CCNT composites have excellent photoelectric properties under visible light.

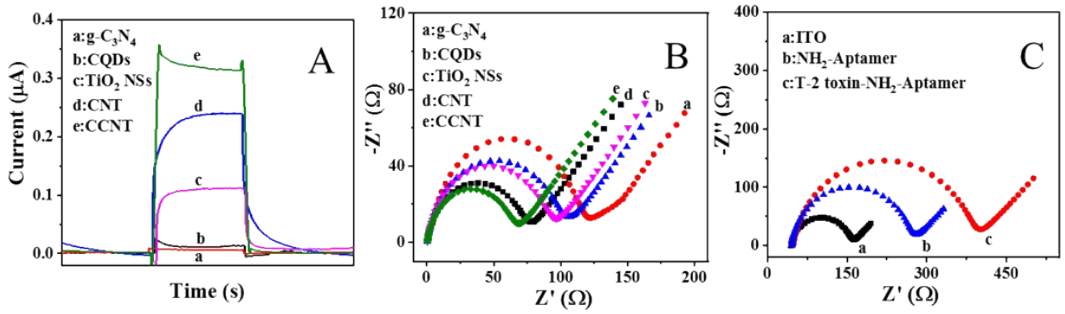

Fig. S5 (A) Photocurrent responses and (B) Electrochemical impedance spectra (EIS) of g-C_3N_4 (a), CQDs (b), TiO_2 NSs (c), CNT (d) and CCNT (e); (C) EIS spectra of ITO (a), NH_2-Aptamer (b) and T-2 toxin-NH_2-Aptamer (c).

Selectivity and reproducibility of the biosensor.

In order to verify whether the method was specific for the detection of T-2 toxin, selective experiments were performed by comparing T-2 with other biotoxins (AFB1, ZEN, OTA and FB1). As shown in Fig. S6A, the fluorescence signal was significantly lower in the presence of 75 ng mL^{-1} T-2 toxin. This apparent difference demonstrated the excellent selectivity of the proposed sensor for T-2 toxin.

The reproducibility of the biosensor was shown in Fig. S6B. Five independent electrodes were used to detect 50 ng mL^{-1} T-2 toxin solution, and they were modified

under the same conditions. The results showed that the responses of the five electrodes were almost the same, and the calculated relative standard deviation (RSD) was 3.1%, indicating that the designed visualized biosensor had good reproducibility.

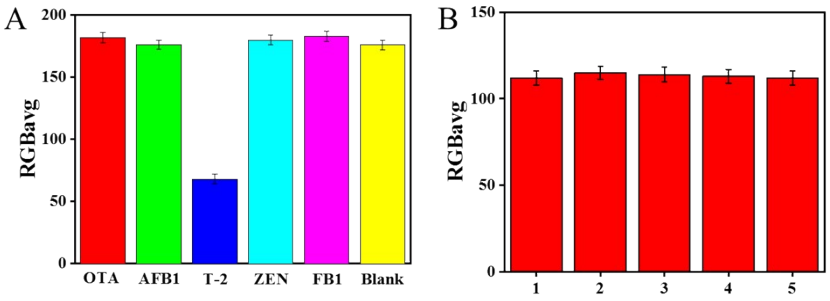

Fig. S6 (A) Specificity of the proposed biosensor platform toward T-2 toxin against other toxins, (B) Stability test of the resulting aptasensor under 5 times test.

Real sample analysis.

The performance of this developed visual biosensor in the actual samples analysis was investigated with beer sample by standard addition methods.[13] A gradient concentration of T-2 toxin was added to the degassed and filtered beer samples. It was found that the recoveries range from 95.0 to 102.8 % (n=3), with the RSD of 3.2-5.3 %, indicating that the biosensor can be used for the detection of T-2 toxin in actual samples, and has a good application prospect in mycotoxins detection (Table S1).

Table S1. Results of T-2 toxin detection in beer samples

Sample	**Added (ng mL^{-1})**	**Found (ng mL^{-1})**	**Recovery (%)**	**RSD (%)**
1	10.0	9.5	95.0	3.2
2	50.0	49.6	99.2	4.8

3	100.0	102.8	102.8	5.3

Table S2. The comparison of different methods for T-2 toxin detection

Analytical Methods	Linear Range	Limit of Detection	References
HPLC-MS/MS	0.05 μg/kg to 100 μg/kg	0.007μg/kg	14
GC-ECD	0.04 $\mu g \cdot mL^{-1}$ to 16 $\mu g \cdot mL^{-1}$	1.88 $ng \cdot g^{-1}$	15
Colorimetric Aptasensor	0.1 $ng \cdot mL^{-1}$ to 5000 $ng \cdot mL^{-1}$	57.8 $pg \cdot mL^{-1}$	16
Fluorescence Aptasensor	0.1 $ng \cdot mL^{-1}$ to 100 $ng \cdot mL^{-1}$	0.087 $ng \cdot mL^{-1}$	17
Fluorescence Visualization	1 $ng \cdot mL^{-1}$ to 100 $ng \cdot mL^{-1}$	0.33 $ng \cdot mL^{-1}$	This work

References

1 S. Zhu, Q. Meng, L. Wang, J. Zhang, Y. Song, H. Jin, K. Zhang, H. Sun, H. Wang and B. Yang, *Angew. Chem. Int. Ed.*, 2013, **52**, 3953-3957.

2 W.-J. Ong, L.-L. Tan, S.-P. Chai, S.-T. Yong and A. R. Mohamed, *Nano Energy*, 2015, **13**, 757-770.

3 X. Han, Q. Kuang, M. Jin, Z. Xie and L. Zheng, *J. Am. Chem. Soc.*, 2009, **131**, 3152-3153.

4 L. Protesescu, S. Yakunin, M. I. Bodnarchuk, F. Krieg, R. Caputo, C. H. Hendon, R. X. Yang, A. Walsh and M. V. Kovalenko, *Nano Lett.*, 2015, **15**, 3692-3696.

5 N. Hao, J. Lu, Z. Dai, J. Qian, J. Zhang, Y. Guo and K. Wang, *Electrochem. Commun.*, 2019, **108**, 106559.

6 T. D. Boone, Z. H. Fan, H. H. Hooper, A. J. Ricco, H. Tan and S. J. Williams, *Anal. Chem.*, 2002, **74**, 78 A-86 A.

7 M. Wei, J. Wan, Z. Hu, Z. Peng and B. Wang, *Appl. Surf. Sci.*, 2016, **377**, 149-158.

8 Y. Li, X. H. Feng, Z. X. Lu, H. Yin, F. Liu and Q. J. Xiang, *J. Colloid Interface Sci.*, 2018, **513**, 866-876.

9 X. Wang, S. Blechert and M. Antonietti, *ACS Catal.*, 2012, **2**, 1596-1606.

10 Z. Lin and X. Wang, *Angew. Chem. Int. Ed.*, 2013, **52**, 1735-1738.

11 M. Liu, H. Li and W. Wang, *Catal. Today*, 2016, **264**, 236-242.

12 R. Boppella, S. T. Kochuveedu, H. Kim, M. J. Jeong, F. Marques Mota, J. H. Park and D. H. Kim, *ACS Appl. Mater. Interfaces*, 2017, **9**, 7075-7083.

13 D. He, Z. Wu, B. Cui, E. Xu and Z. Jin, *Food Anal. Meth.*, 2019, **12**, 625-632.

14 Z. Zou, Z. He, H. Li, P. Han, J. Tang, C. Xi, Y. Li, L. Zhang and X. Li, *Meat Sci.*, 2012, **90**, 613-617.

15 W. J. Kong, X. F. Zhang, H. H. Shen, Z. Ou-Yang and M. H. Yang, *Food Chem.*, 2012, **132**, 574-581.

16 Z. Qie, W. Yan, Z. Gao, W. Meng, R. Xiao and S. Wang, *Microchim. Acta*, 2019, **186**, 816.

17 X. D. Zhao, Y. Wang, J. Z. Li, B. Y. Huo, H. Huang, J. L. Bai, Y. Peng, S. Li, D. P. Han, S. Y. Ren, J. Wang and Z. X. Gao, *Anal. Chim. Acta*, 2021, **1160**, 10.